Enthesis trauma as a means for the development of translatable chronic rotator cuff degeneration in an ovine model

James Johnson[1]^, Devin von Stade[1]^, Daniel Regan[2]^, Jeremiah Easley[3], Lyndah Chow[4]^, Steven Dow[2,4], Tony Romeo[5], Ted Schlegel[6], Kirk McGilvray[1]^

[1]Orthopaedic Bioengineering Research Laboratory, Colorado State University, Fort Collins, CO, USA; [2]Flint Animal Cancer Center and Department of Microbiology, Immunology, & Pathology, CSU Flint Animal Cancer Center, Fort Collins, CO, USA; [3]Preclinical Surgical Research Laboratory, Colorado State University, Fort Collins, CO, USA; [4]Department of Clinical Sciences, Center for Immune and Regenerative Medicine, Colorado State University, Ft. Collins, CO, USA; [5]Rothman Orthopaedic Institute, New York, New York, USA; [6]Department of Orthopedics/ University of Colorado School of Medicine, Aurora, CO, USA

Contributions: (I) Conception and design: All authors; (II) Administrative support: All authors; (III) Provision of study materials or patients: All authors; (IV) Collection and assembly of data: All authors; (V) Data analysis and interpretation: All authors; (VI) Manuscript writing: All authors; (VII) Final approval of manuscript: All authors.

Correspondence to: Kirk McGilvray, PhD. 1374 Campus Delivery, Fort Collins, CO 80523, USA. Email: kirk.mcgilvray@colostate.edu.

Background: Untreated rotator cuff tears lead to irreversible tendon degeneration, resulting in unacceptable repair prognosis. The inability of current animal models of degenerated rotator cuff tendons to more fully emulate the manifestation and degree of pathology seen in humans with a previously torn rotator cuff tendon (s) significantly impairs the development of novel therapeutics. Therefore, the objective of this study was to develop a large-animal translational model of enthesis damage to the rotator cuff tendons to mimic the chronic degenerative changes that occur in patients that demonstrate clinical manifestations of tendinopathy.

Methods: A partial enthesis tear model (i.e., sharp transection) in adult sheep was created by cutting the tendon fibers perpendicularly through the enthesis midpoint, while leaving the other portion of the tendon in-tact. To assess tendon integrity, non-destructive biomechanical tests were performed, followed by histopathological, histomorphological, and gene expression analysis. Samples of degenerated human rotator cuff tendons obtained from patients undergoing reverse total shoulder arthroplasty to use for comparative pathological analysis.

Results: In the sheep model, transected tendons at all timepoints had significantly decreased mechanical properties. Histopathologic evaluation and Bonar scoring revealed that the tendons in sheep underwent degenerative changes similar in magnitude and manifestation as the degenerated human tendon samples. Furthermore, similar levels of collagen disorganization were noted between the 6 and 12-week ovine samples and the degenerated human samples.

Conclusions: These findings indicate that the new sheep model of rotator cuff injury reliably recapitulates the structural and cellular changes that occur clinically in humans with chronic rotator cuff tendon injuries and suggest that this new model is well suited to evaluation of new therapeutic interventions.

Keywords: Rotator cuff, chronic degeneration, histopathology, biomechanics, gene expression

^ ORCID: James Johnson, 0000-0001-7465-3854; Devin von Stade, 0000-0002-2617-8283; Daniel Regan, 0000-0002-3148-1332; Lyndah Chow, 0000-0002-6413-9517; Kirk McGilvray, 0000-0003-1302-9307.

Page 2 of 15

Johnson et al. Translatable model of chronic rotator cuff degeneration

Introduction

The rotator cuff is a group of tendons in the shoulder that is responsible for stability and motion of the arm; tears to these tendons can cause pain, instability, and an inability to perform day-to-day tasks. Previous studies of cadaveric shoulders have found that 18.5% of the general population has at least partial tears of rotator cuff tendons (1,2). As these partial tears do not typically result in significant impairment of the arm, conservative treatment is generally implemented in lieu of surgical repair (3). However, growing clinical and basic science evidence suggests that these partial tears result in a deleterious degenerative cascade of the rotator cuff tendon/muscle group, leading to fatty infiltration, loss of muscle strength, and most importantly, increased probability of full thickness tears at a later point in life (4,5). Additionally, this chronic degeneration of the tendon(s) (a.k.a., tendinopathy) has a negative impact on the clinical outcome of repair surgeries on torn tendons, with re-tear rates of arthroscopic repairs as high as 94% depending on exacerbating risk factors (6-9).

The etiology of chronic tendon degeneration is complex, and the mechanistic underpinnings are not yet fully understood. Chronic degeneration is known to entail several pathological changes in tendons, including a proliferation of tenocytes, excess proteoglycan content, disorganized collagen fibers, and increased vascularization (10-13). Changes are not limited to the tendon tissue; marked fatty infiltration of the associated muscle groups is another hallmark of rotator cuff degeneration. There is no consensus on a single underlying cause leading to chronic rotator cuff degeneration, but it is hypothesized that the degeneration cascade stems from factors such as overuse or history of tendon injury (i.e., previous partial width tears) (14,15).

The poor prognosis and high frequency of rotator cuff damage necessitates continued research into new surgical techniques and therapeutics to improve upon currently inadequate clinical outcomes. A variety of translational comparative animal models (e.g., murine, leporine, canine, ovine, and non-human primates) have been used in attempts to simulate the human degeneration cascade; however, none have been able to faithfully recapitulate the broad spectrum of changes that are seen in humans (16-20). Furthermore, the inherently small size of some of these animal models (i.e., 'small animals') precludes the assessment of physiologically-relevant sized devices or comparable dosages of cellular therapies intended for use in humans. This has led some researchers to propose the use of ewes as a translational

model for rotator cuff injury (21-23). One of the first ovine models used as a means to generate degenerative changes to tendons in the rotator cuff involved a full transection of the infraspinatus tendon with a delayed repair (24). While this model was considered the gold-standard for some time (24-26), it has since been demonstrated that this model leads to severe tendon retraction, which is not observed clinically and results in repair surgery complications (27). To overcome this shortcoming, a partial transection model in which half of the infraspinatus' width was transected from the enthesis, followed by a delayed repair was created (18,22,28,29). Unfortunately, this model was also found to create pathologic changes that are best described as an acute reparative injury process (amplified tenocyte reactivity, neo-vascularization, and inflammation), in contrast to what has been noted clinically in patients with tendinopathy (22,30).

Considering the inability of the current large-animal translational models to accurately replicate the chronic, degenerated human condition [i.e., haphazard collagen organization, increased cellularity, increased vascularity, etc. (13)], there is a clear need to explore new models that can more closely replicate the magnitude and characteristics of the human tendon degeneration cascade. Therefore, the purpose of this study was to investigate a novel ovine model of chronic rotator cuff degeneration. We hypothesized that surgically induced damage at the tendon-bone enthesis (i.e., sharp surgical transection through 50% of the enthesis; akin to a partial tear), while still leaving the entire width of the tendon attached, would initiate a degree of degeneration which parallels that observed in degenerated human tendons clinically, as evidenced by comprehensive biomechanical, histopathological, histomorphological, and gene expression analyses. The rational for this approach was that by leaving the entire width of the tendon attached (as opposed to previous full or partial transection models), the severity of pathologic changes would more closely match what has been documented in human cases. We present the following article in accordance with the ARRIVE reporting checklist and the MDAR checklist (available at http://dx.doi.org/10.21037/atm-21-354).

Methods

Human tissue collection

The study was conducted in accordance with the Declaration of Helsinki (as revised in 2013). The study was approved by institutional ethics board of the Rush Medical

University (NO.: 16110707-IRB01) and informed consent was taken from all individual participants.

Human supraspinatus tendon tissue (10 mm × 20 mm; length × width) was obtained from seventeen patients (n=17 samples) undergoing primary reverse shoulder arthroplasty (PRSA). Inclusion criteria were that the patients were undergoing PRSA and had indications of chronic, degenerative rotator cuff tendinopathy. PRSA was performed on arthritic patients with well documented chronic rotator cuff injuries. Succinctly, the rotator cuff injuries in these patients are often severe and the tendons exhibit symptoms of chronic degeneration that would prohibit normal shoulder motion if a normal arthroplasty were performed (31,32). Due to the severe level of degeneration, portions of rotator cuff tendons must be removed, enabling tissue collection for this study. This patient cohort had an age of 68±7 years, all demonstrated clinical signs of chronic tendon degeneration [i.e., MRI assessment of tendon injury including fatty infiltration of the associated muscles (33)] and some having histories of previously failed rotator cuff tear (RCT) repair surgeries (6 out of 17 patients). Tissue samples were collected intra-operatively and were placed in 10% neutral buffered formalin for fixation at the time of collection. Collected and fixed samples were allocated to histopathologic assessment. Due to the small size of tissue biopsies, it was deemed infeasible to mechanically test the human tissue samples. Previously published gene expression data from human subjects with chronic tendon degeneration was used as a representative population for genetic expression comparisons (34).

Ovine model—surgical procedures

Experiments were performed under a project license (NO.: 18-7854A) granted by institutional committee board of Colorado State University, in compliance with United States national or institutional guidelines for the care and use of animals.

Bilateral surgical damage was created to the infraspinatus tendons in twenty skeletally mature (≥3.5 years of age) *Ovis aries* ewes resulting in n=40 treated shoulders. Rams were not utilized in this study due to husbandry difficulties and aggressive behavior. The sheep were prepared for bilateral surgery and placed in dorsal recumbency under general anesthesia. The surgical models [model 1: sharp partial transection of the entheses (n=20 treated shoulders); model 2: combed fenestration of the enthesis and tendon mid-

substance (n=20 treated shoulders—data intentionally omitted from this manuscript so that it can be compiled into a standalone publication)] were alternated between shoulders to eliminate the potential of a left/right side bias.

A standard surgical preparation and approach was followed; the *m. subcutaneous coli* was divided in line with the incision, and the *m. deltoideus* was split along the tendinous division between the heads of the acromion and scapula. The superficial head and insertion of the infraspinatus tendon was isolated, followed by creation of the surgical insult. The enthesis damage model, "sharp transection" (ST), was generated by cutting the tendon fibers perpendicularly through the midportion of the attachment site on the humerus (i.e., the footprint) (*Figure 1*). This was done to simulate damage at the tendon insertion that does not result in a complete separation of the tendon from the humerus, similar to what is hypothesized to occur in humans that have suffered a partial thickness tear at the enthesis. Following model generation, standard surgical closure procedures were followed. The sheep were allowed to eat and ambulate *ad libitum* during convalescence. Sheep were monitored daily throughout the study period for any signs of adverse events or complications and to evaluate pain, lameness/ambulatory function, and incisional site healing.

Animals were humanely euthanized at 6, 12, and 18 weeks to capture the time-mediated tissue response to injury and degeneration. The humerus-infraspinatus tendon constructs (HTCs) were immediately harvested following euthanasia. Six uninjured shoulders were harvested from sheep utilized in unrelated studies to use as controls. HTCs were isolated and denuded of soft tissues with great care as to not damage the infraspinatus tendon. A small portion (5 mm × 20 mm, width × length) of tendon on the caudal/ventral side was taken immediately upon dissection and snap frozen in liquid nitrogen to be used for RNA sequencing. Pilot experiments (data not shown) demonstrated that RNA biopsy collections did not compromise the mechanical competency of the tendon.

Biomechanical testing

Three cross-sectional area (CSA) measurements of all tendons were taken proximal to the insertion using previously validated techniques in which an area micrometer that applied 0.12 MPa of pressure parallel to the cross section of the tendon (23,35-37). The minimum of these CSA measurements was used to transform force to stress,

Page 4 of 15

Johnson et al. Translatable model of chronic rotator cuff degeneration
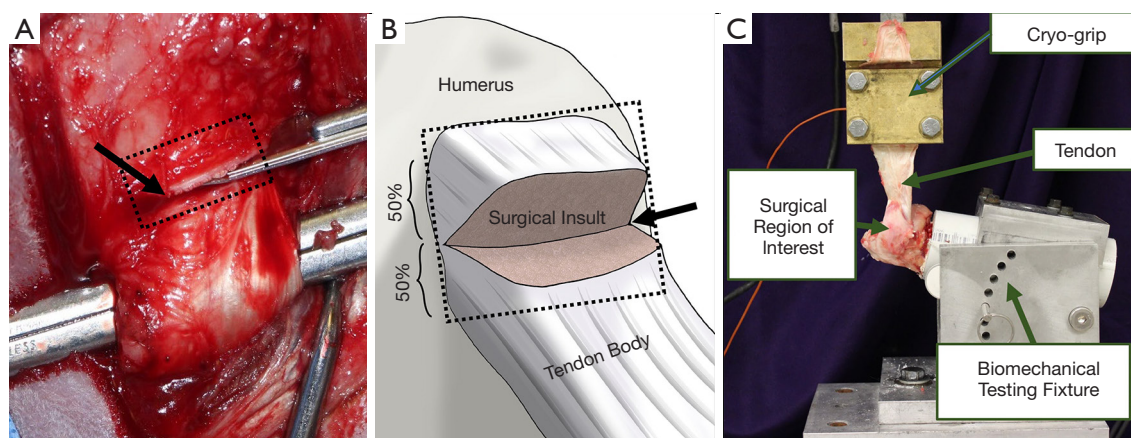
Figure 1 Model generation and biomechanical testing setup images. Intra-operative image illustrating location of surgical insult at the midpoint of the tendon insertion (A) and digital illustration of surgical insult and relevant tissue (B). Rectangular box outlines the tendon insertion, arrow highlights the surgical cut. Image of biomechanical testing (C).

resulting in values that indicate the highest level of stress in each tendon. For purposes of reporting tendon overall CSA, these measurements were averaged. The humeri were subsequently mounted in polyvinyl chloride (PVC) sleeves using a strong two-part hard casting resin (SmoothCast 321, Smooth-On, Macungie, PA) and mounted in a custom fixture attached to a servo-hydraulic load frame (Model 805, MTS Corp., Eden Prairie, MN) which allowed anatomically accurate loading of the tendon (*Figure 1*) (23,25). Prior to biomechanical testing, tendons underwent a pre-loading phase to normalize viscoelastic effects in which a static preload of 5N was applied for a duration of two minutes (37-42). Gage length of the tendon was measured at the end of the preload period, allowing transformation of the testing data from displacement to stretch. Non-destructive stress relaxation tests were then performed for 100 seconds at physiologically relevant stretch levels of 1.06 and 1.08 (41,43), with peak stress (MPa), peak force (N), and percent relaxation (%) being measured (44). Recovery periods of 1,000 seconds between tests were implemented to allow samples to come to viscoelastic equilibration (41). Tendon hydration was maintained with physiological saline during the entire preparation and mechanical testing procedure.

Histological analysis

Immediately following mechanical testing, samples were removed from their potting sleeves and bisected through the enthesis to improve infiltration of the fixative agent (23). These humerus-infraspinatus tendon constructs were then fixed in 10% neutral buffered formalin (≥7 days), demineralized in 8% trifluoroacetic acid, embedded in paraffin, sectioned at the mid-tendon-body, and mounted on a glass slide., Two 5 μm thick slides were cut from each sample; one slide was stained with hematoxylin and eosin (H&E) and the other slide was stained with Picro-Sirius red.

H&E slides were graded by a blinded veterinary pathologist in residency using the semiquantitative Bonar tendinopathy scale via bright-field and polarized light microscopy assessing: (I) tenocyte reactivity, (II) angiogenesis, (III) tendon bundle organization and polarization, and (IV) deposition of ground substance (45). Each of these four characteristics were graded on a 4-point scale ranging from 0 (normal/healthy) to 3 (markedly "degenerated"/pathologic) (45). These scores were then summed to give an overall score between 0 (pathologically normal) and 15 (pathologically degenerated) for each tendon section.

Histomorphological assessment of collagen fiber alignment

Picro-Sirius red stained slides were utilized to assess collagen fiber organization in all ovine and human tissues. Slides contained 40 mm of the proximal infraspinatus tendon and enthesis/bone were prepared and imaged using polarized brightfield microscopy at 2× magnification (Olympus BX61VS, Center Valley, PA). All samples were imaged in one session with 40ms exposure to ensure no variation in imaging capture process or polarization lens configuration. Commercially available software (Image-Pro

Plus, RRID:SCR_007369) was used to calculate percent area of the organized/disorganized collagen seen within the injury region of the tendon. Region of analysis included the most proximal 25 mm of tendon but did not include the fibrocartilaginous enthesis zone. To ensure the accuracy of the program the veterinary pathologist in residency verified the algorithm's ability to differentially identify organized and disorganized regions of collagen for a subset of samples.

RNA sequencing

Tendon samples for gene expression analysis were taken immediately during fine dissection and flash frozen in liquid nitrogen to prevent RNA degradation. Tendon samples were pulverized then lysed (TRizol™ Invitrogen, Carlsbad, CA) to enable precipitation of RNA followed by purification using chloroform method as previously described (46) with increased incubation time to account for the size of the tendon biopsy. Commercially available kits (RNeasy, Qiagen, Hilden, Germany) were then used to purify extracted RNA following manufacture protocol.

Frozen RNA samples were sent to a commercial genomics center (Novogene Inc., Sacramento, CA) for quality analysis and sequencing. RNA quality was verified by electrophoresis (2100 Bioanalyzer Instrument, Agilent, Santa Clara, CA). The cDNA library was constructed with a commercially available kit following manufactures instructions (Ribo-Zero, Illumina, San Diego, CA). Paired end reads were obtained (HiSeq 2500, Illumina, San Diego, CA), and gene expression data were processed using a statistical and visualization analyses package (Partek Genomics Suite, RRID:SCR_011860). After adapter trimming and filtering for Phred score >20, paired end reads were aligned to Oar_v3.1 genome assembly using TopHat (47). Gene counts were obtained using Partek E/M annotation model. Differentially expressed genes were calculated for each timepoint compared to uninjured samples using Partek GSA (gene specific analysis) and non-parametric ANOVA.

Statistical analysis

All comparisons between groups were made using a one-way ANOVA followed by Fisher's post-*hoc* test (Minitab, RRID:SCR_014483). All data passed Anderson-Darling normality test. Data that did not pass Levene test for equal variance were transformed with Box Cox transformation. Final sample sizes were chosen to achieve 80% statistical power using results from pilot animals. Sample numbers in each grouping were: n=6 shoulders at the 6- and 12-week timepoints, n=8 shoulders at the 18-week timepoint, and n=6 shoulders for the uninjured control group. Ewes were randomly assigned to sacrifice timepoints. No specimens/samples were excluded from this study. Correlation analysis were performed, results of Pearson correlation coefficients and associated P-values were reported.
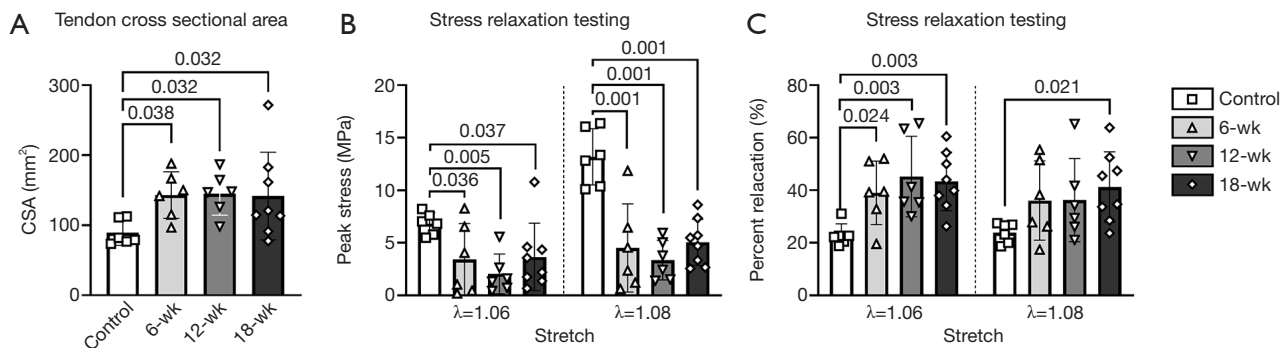
Results

All twenty animals survived to the 6, 12, and 18-week timepoints. No intra- or post-operative complications were noted.

Mechanical Testing

There were marked, significant increases in CSA at all timepoints as compared to the uninjured control group with the ST tendons exhibiting increases in CSA of 60.3% (P=0.038), 62.5% (P=0.032), and 58.8% (P=0.032) at the 6, 12, and 18-week timepoints, respectively (*Figure 2*). Additionally, the ovine tendons that underwent sharp transection demonstrated decreased biomechanical properties (*Table 1*). At all timepoints the injured tendons exhibited marked, significant reductions in peak stress at both stretch levels (*Figure 2*), with the ST tendons exhibiting decreases of: 50.0% (6-wk, λ=1.06, P=0.036), 65.9% (6-wk, λ=1.08, P=0.001), 69.1% (12-wk, λ=1.06, P=0.005), 74.2% (12-wk, λ=1.08, P=0.001), 45.6% (18-wk, λ=1.06, P=0.037), and 61.4% (18-wk, λ=1.08, P=0.001). The viscous response of the tendons was also altered, with increases in percent relaxation (as compared to uninjured) at both stretch magnitudes (*Figure 2*), with the ST tendons exhibiting decreases of: 69.6% (6-wk, λ=1.06, P=0.024), 51.7% (6-wk, λ=1.08, P=0.115), 96.5% (12-wk, λ=1.06, P=0.003), 52.5% (12-wk, λ=1.08, P=0.110), 88.7% (18-wk, λ=1.06, P=0.003), and 73.1% (18-wk, λ=1.08, P=0.021).

Histopathology results

In contrast to the uninjured ovine samples (*Figure 3A*), the sharply transected ovine tendons (*Figure 3B,C,D*) exemplified pathological degeneration characteristics of human tendinopathy (*Figure 3E*). There was marked disruption of the superficial tendon abutting or adjacent to the enthesis in this ovine model. These changes in the ovine model were further characterized by loss of lamellar

Page 6 of 15

Johnson et al. Translatable model of chronic rotator cuff degeneration

Figure 2 Biomechanical testing results. Tendon cross-sectional area (CSA) measurements (A). Peak stress from the stress-relaxation testing at both stretch levels (B). Percent relaxation from the stress-relaxation testing at both stretch levels (C). P values are indicated for all pairwise comparisons which met the significance threshold ($P<0.05$).

Table 1 Biomechanical and geometric properties for tendon samples

Timepoint	Stretch	Percent relaxation (%)	P value	Peak load (N)	P value	Peak stress (MPa)	P value	Area (mm^2)	P value
Control	$\lambda=1.06$	23.00±3.90	–	582±101	–	6.8±1	–	89±16	–
	$\lambda=1.08$	23.80±3.50	–	1,108±161	–	13.2±2.4	–		–
6 Weeks	$\lambda=1.06$	39.00±11.00	0.024	438±372	0.378	3.4±3.1	0.036	143±30	0.038
	$\lambda=1.08$	36.10±13.70	0.115	564±396	0.003	4.5±3.8	0.001		
12 Weeks	$\lambda=1.06$	45.20±14.00	0.003	281±228	0.073	2.1±1.7	0.005	145±28	0.032
	$\lambda=1.08$	36.30±14.40	0.11	457±269	0.001	3.4±1.7	0.001		
18 Weeks	$\lambda=1.06$	43.40±10.40	0.003	342±246	0.122	3.7±3	0.037	142±59	0.032
	$\lambda=1.08$	41.20±12.60	0.021	490±137	0.001	5.1±2	0.001		

Data are shown as means ± SD. $P<0.05$ indicate difference with uninjured control group at same stretch level.

bundle organization, marked expansion of tenoblast (a.k.a., immature tenocyte) populations (*Figure 3*, square), and deposition of ground substance (*Figure 3*, arrow) which all contribute to the expansion of the tendon thickness. Tenoblasts rarely form lacunae (*Figure 3*, triangle) suggestive of early chondroid metaplasia. Arising from the superficial, adjacent humeral head and overlying this area of the tendon was a variably thick band of dense granulation tissue with prominent angiogenesis that extended into the tendon body. At times capillary clusters were prominent throughout the tendon body but were always most dense within the area of injury and the overlying granulation tissue (*Figure 3*, diamond). There is variable enthesophyte formation at the superficial enthesis.

Biopsies of human supraspinatus tendon body were comprised of dense connective tissue demonstrating similar histologic features to the ovine sharp transection model

adjacent to the site of injury. There was severe loss of lamellar collagen bundle organization and expansion of tenoblast populations (*Figure 3*, square) with rare lacunae formation, increased numbers of capillary profiles (*Figure 3*, diamond) and moderate amounts of ground substance (*Figure 3*, arrow) separating collagen bundles.

Results of the semi-quantitative Bonar scoring for tendon degeneration characteristics are summarized in *Figure 4*. At all timepoints the ST ovine model and the degenerated human samples scored significantly higher than uninjured ovine samples [8.67 ($P<0.01$), 8.83 ($P<0.01$), and 9.38 ($P<0.01$), for the 6, 12, and 18-week timepoints, respectively].

Histomorphological assessment of collagen fiber alignment

The surgical disruption of the enthesis resulted in marked
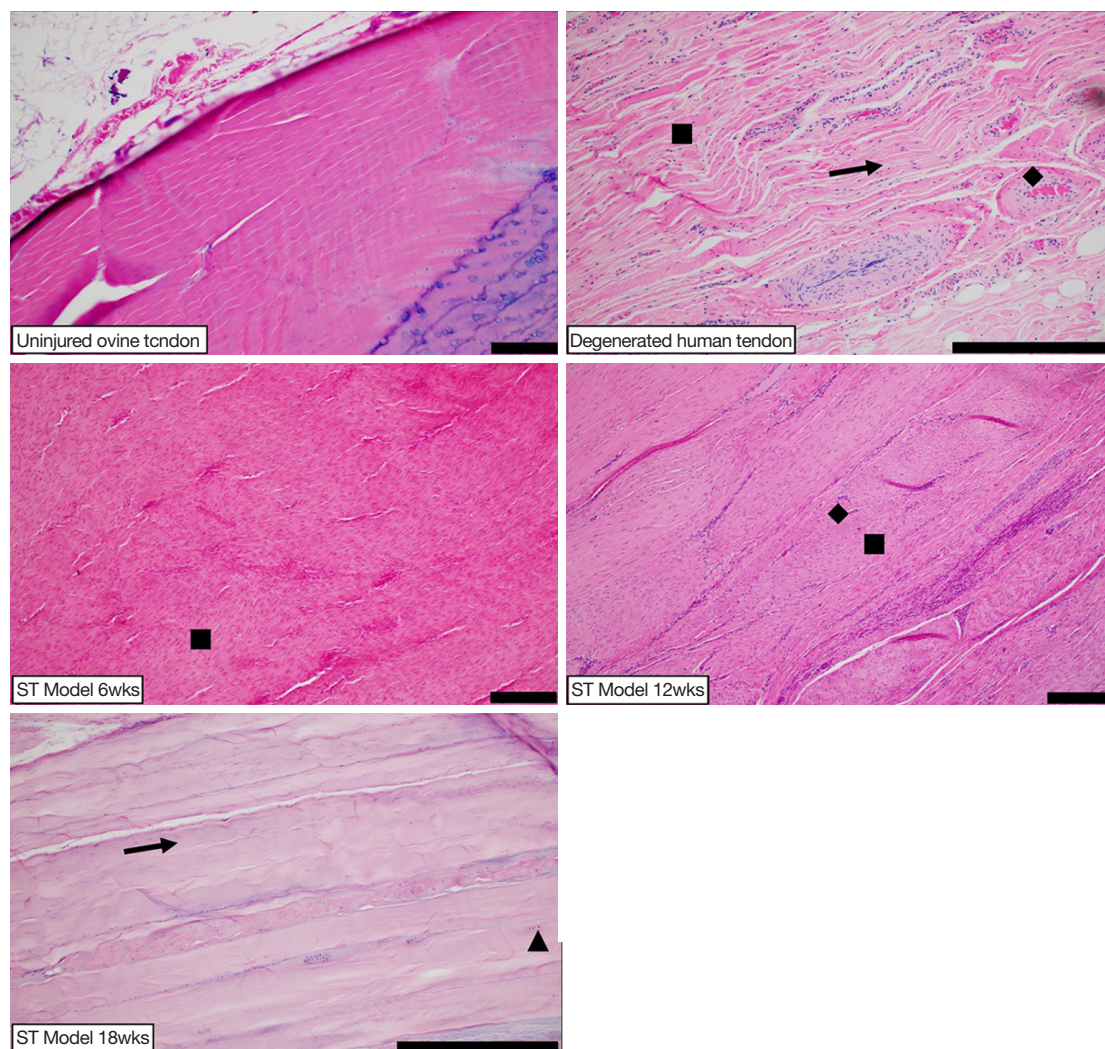
Figure 3 For each image, the black scale bars on the bottom right corner of the image are 500 μm. Representative micrographs of H&E stained slides for all tendon groups. Marked increase of tenoblast population throughout tendon body with indicator at representative areas (square). Deposition of ground substance (arrow). Tenoblasts within lacunae (triangle). Increased vascularization (diamond).

disorganization of collagen fibers throughout tendon in the ST model. Analysis of the amount of organized collagen fibers revealed marked decrease in organization in both the human and ST tendon samples (*Figure 4*), with reductions (as compared to the uninjured ovine group) of 51.0% (P=0.001), 25.7% (P=0.071), 4.4% (P=0.738), and 37.1% (P=0.002) for the 6-week ST, 12-week ST, 18-week ST, and degenerated human groups, respectively.

RNA sequencing

To investigate the gene expression profile changes related to the ovine tendon injury cascade, RNA sequencing was performed on two or three tendon biopsies per time point (12-week n=3, 16-week n=3, 18-week n=2). RNA-seq revealed gene expression patterns consistent with tendon degeneration over the entire 18-week observation period. Analysis of the resultant principal component analysis (PCA) plot, which depicts the differences in the 17,230 transcripts found using spatial positioning; the 12-week samples appear to be the most divergent from the control group (uninjured ovine) (*Figure 5A*). Specifically, the significantly upregulated genes increased from 164 at 6 weeks post-surgery (*Figure 5B*), to 226 at 12 weeks (*Figure 5C*), and vastly increase again to

Page 8 of 15

Johnson et al. Translatable model of chronic rotator cuff degeneration
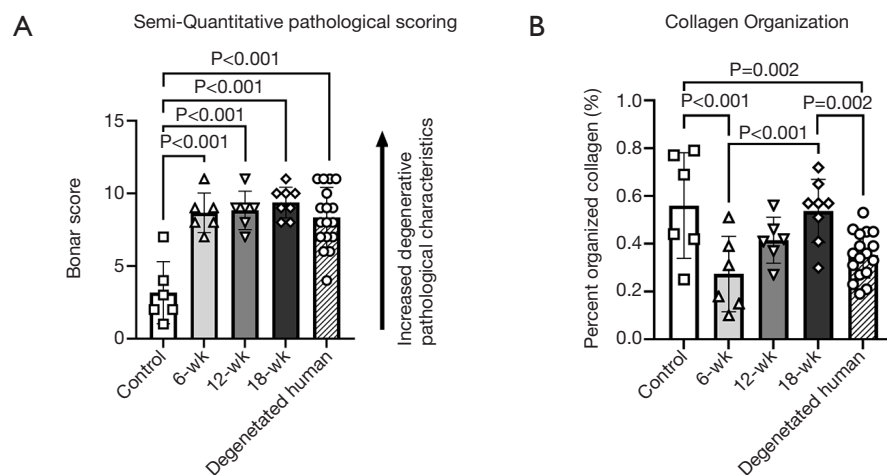
Figure 4 Tendon pathology and collagen organization. (A) Overall Bonar degeneration score calculated by summing semi-quantitative scoring in the following categories: tenocytes, ground substance, collagen, and vascularity. (B) Area of organized collagen normalized to total region analyzed as measured with polarized light microscopy and Picro-Sirius red staining. P values are indicated for all pairwise comparisons which met the significance threshold (P<0.05).

937 at 18 weeks (*Figure 5D*).

Gene Ontology of Biological Processes (GO BP) was assessed to document gene set enrichment that may be used for comparison in future studies. RNA gene counts were tabulated, grouped by time point and run in GSEA (gene set enrichment analysis software version 4.1.0) using the GO_BP gene set (version 7.2). Each time point was challenged with the uninjured group individually (i.e., 6-week ST *vs.* uninjured) and as a pooled "injured" group (i.e., all ST samples *vs.* uninjured). The top 30 normalized enrichment scores with false discovery rates less than 5% (FDR-q <0.05) were selected from each data set for graphical analysis (*Figure 6*). Gene sets were grouped by shared biological process ontology categories [Mouse Genome Informatics (MGI), RRID:SCR_006460].

Correlation analysis

Significant correlations were observed between gene expression, mechanical testing, and pathologic scoring data. To compare the RNA-seq results to the mechanical testing and tendon pathology, 172 genes were selected for changes in expression levels present throughout the 18-week timepoints (*Table 2*). Temporal gene expression levels in RPKM (reads per kilobase transcript) were compared to Bonar score, collagen organization, CSA, maximum stress, and percent relaxation. There were significant gene expression correlation results (22 genes) found with

collagen organization, percent relaxation, and Bonar scoring as shown in *Table 2*, all of which are protein coding genes. Several of the gene correlations with Bonar score had Pearson coefficients with magnitudes greater than 0.7: TRIM11 (ρ=0.774, P=0.01), PCDHGA1 (ρ=−0.772, (P=0.01), and THAP1 (ρ=0.724, P=0.01), indicating that the RNA sequencing was able to illuminate some of the underlying cellular pathways associated with tendinopathy.

The mechanical properties were also compared to the pathologic criteria. The Bonar score was found to be strongly and significantly correlated with the peak stress (λ=1.08) of the tendons (ρ=−0.72, P<0.01, *Figure 7*), percent relaxation (λ=1.08, ρ=0.49, P=0.01), and CSA of the tendons (ρ=0.51, P<0.01). The peak stress was strongly and significantly correlated with the CSA of the tendons (λ=1.06: ρ=−0.68, P<0.01; λ=1.08: ρ=−0.76, P<0.01; *Figure 7*) and the ratio of organized collagen at both stretch magnitudes (λ=1.06: ρ=0.48, P=0.01; λ=1.08: ρ=0.42, P=0.03).

Conclusions

Several ovine models have been attempted in an effort to emulate the degenerative changes seen in humans clinically (22,24,29). Unfortunately, these models have led to degenerative changes that did not fully match the severity or form of what has been noted in humans. In contrast to the previous models, this new model of controlled enthesis injury was able to produce similar levels of tenocyte
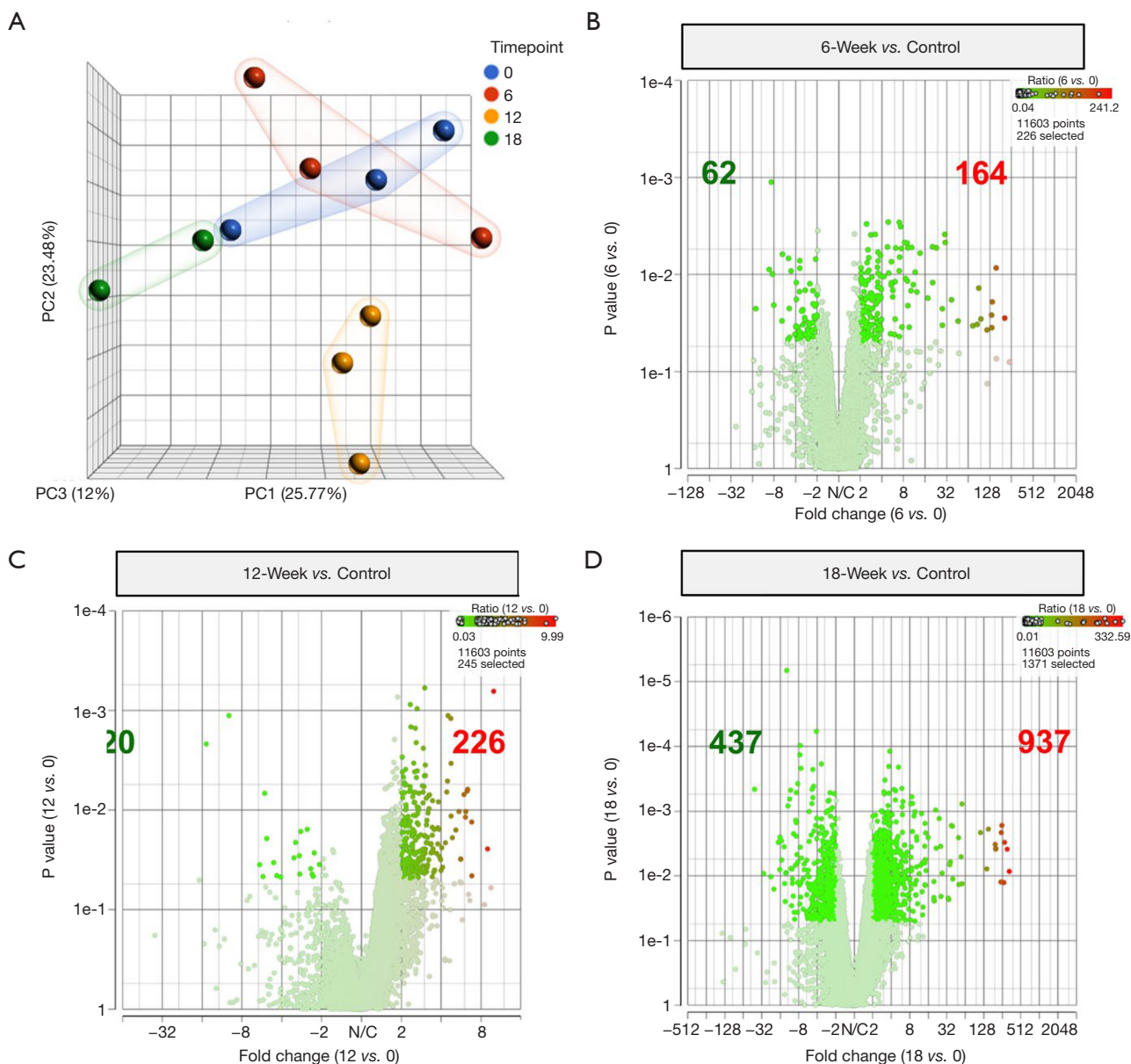
Figure 5 Gene expression changes in Tendon following sharp transection. (A) PCA plot illustrating the gene expression variance between the different timepoints of the Sharp Transection model and uninjured. Same time points grouped according to color (legend shown in top right corner). (B) Volcano plot comparing 12-week gene expression count to uninjured. X axis shows fold change y axis shows P value. Significant genes with P value <0.05 and fold change >2 or <−2 shown in bright red and green gradient with ratio scale on top right. At the 6-week timepoint, there were 164 significantly upregulated genes and 62 significantly downregulated genes. (C) Volcano plot comparing 16-week gene expression count to uninjured. 225 significantly upregulated genes and 20 significantly downregulated genes. (D) Volcano plot comparing 18-week gene expression count to uninjured. 937 significantly upregulated, 437 significantly downregulated.

reactivity, angiogenesis, collagen organization, and ground substance deposition that were hallmarks of the degenerated human sample group. These changes were measured through both the histomorphometric quantification of

organized collagen and the semiquantitative pathologic scoring. This model has also demonstrated inferior mechanical properties, thus highlighting the multimodal manifestation of degenerative-like changes. These changes

Page 10 of 15

Johnson et al. Translatable model of chronic rotator cuff degeneration
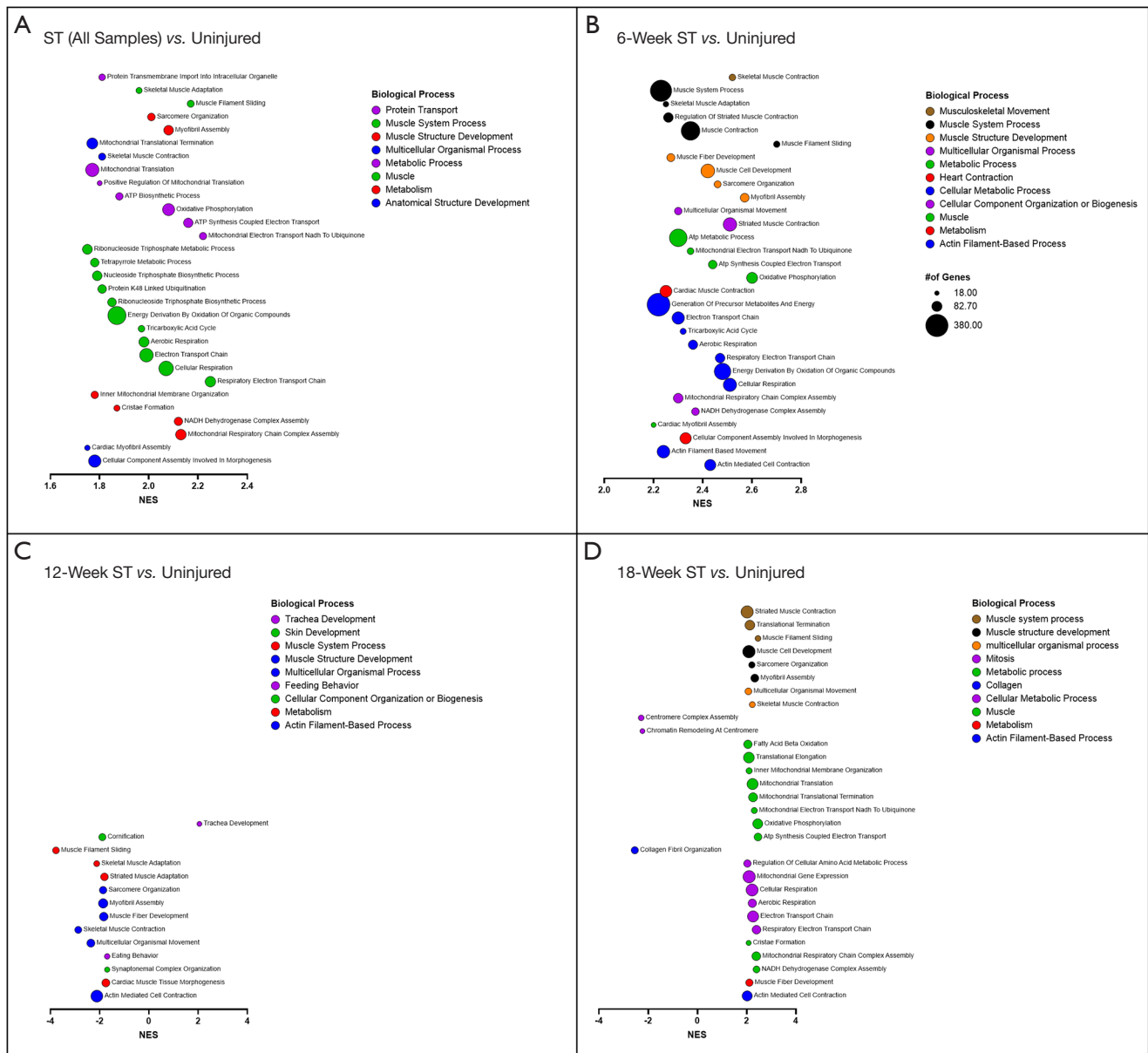
Figure 6 GSEA analysis of gene expression changes following sharp transection. Bubble plot illustrating results of GSEA using the GO BP gene set. The top 30 gene sets by normalized enrichment score (NES) (FDR-q <0.05 and NOM-p <0.01) of the following analyses are shown: all ST *vs.* uninjured (A), 6-week ST *vs.* uninjured (B), 12-week ST *vs.* uninjured (C), and 18-week ST *vs.* uninjured (D). Bubble colors correspond to biological process category, bubble size according to gene count, and bubble location according to NES.

were still witnessed at the latest timepoint, 18-weeks. This suggests that the changes occurring in these tendons are long-term and lead to a similar cascade of changes that are used to describe chronic degeneration of human RCT.

These data presented above highlight the deteriorations in mechanical performance of the ST tendons at all
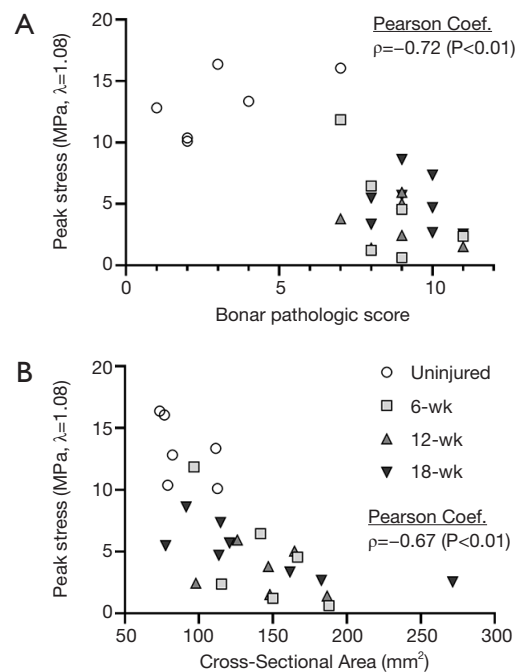
timepoints, as illustrated by both peak stress and percent relaxation. Multiple groups have performed destructive testing on ovine infraspinatus tendons and reported decreases in ultimate load between 2,754.3 N (78.3%) (25) and 3,301.2 N (78.4%) (48) for acutely repaired tendons as compared to intact tendons. Similar results have been

Table 2 Correlation of changes in gene expression with mechanical testing results and pathological characteristics

	Gene ID	ρ	P value
Col. Org. (%)	*LRRC25*	–0.664	0.03
Percent Relaxation (%, λ=1.08)	*ANKRD34A*	0.662	0.03
	SSUH2	0.646	0.03
	FGB	0.684	0.02
Bonar Score	*TRIM11*	0.774	0.01
	THAP1	0.724	0.01
	SLC16A10	0.692	0.02
	PAQR8	0.682	0.02
	CAPN15	0.680	0.02
	URM1	0.680	0.02
	COMMD4	0.671	0.02
	DOK2	0.667	0.03
	RHOF	0.663	0.03
	NUP210	0.655	0.03
	CD274	0.650	0.03
	MAP4K1	0.632	0.04
	IL18R1	0.630	0.04
	CYTIP	0.626	0.04
	SLC6A17	–0.615	0.04
	FGFR3	–0.632	0.04
	PKDREJ	–0.684	0.02
	PCDHGA1	–0.772	0.01

172 genes were selected from 6-, 12-, and 18-week time points compared to uninjured control, based on a fold change of >2 or <–2. For n=11 sheep, gene expression in RPKM was compared to numerical values of mechanical scoring. Significant values were filtered out based on P<0.05 in correlation analysis. This table shows list of genes with high correlation to mechanical testing categories in collagen organization, percent relaxation, and Bonar degeneration score.

Figure 7 Correlation plots. (A) Scatterplot illustrating the relationship between the non-destructive biomechanical response of the tendons as related to the pathologic degeneration scoring. Peak stress was markedly and significantly decreased in samples that evidenced increased pathologic characteristics (ρ=−0.72, P<0.01). (B) Scatterplot illustrating the relationship between the non-destructive biomechanical response of the tendons and their respective cross-sectional areas. Peak stress was markedly and significantly decreased in samples with increased CSA (ρ=−0.67, P<0.01).

reported in a canine repair model; Derwin *et al.* reported a reduction in ultimate force of 927 N (58.1%) (28). Unfortunately, direct comparisons between destructive and non-destructive biomechanical testing are not valid, the results of these studies lend credence to our data indicating decreased mechanical performance associated with injury and deterioration. Furthermore, Derwin *et al.* reported between 84% and 303% increase in CSA of the canine

tendons at 6 and 12 weeks, respectively. This increase in CSA which was noted at all timepoints in the ST tendons.

Histopathologic changes for this ST model demonstrate similar pathology to what was previously described in people (13,49-51). Translatable changes include those defined in the semi-quantitative Bonar scoring (*Figure 4*). Collagen disruption was marked, with mild cartilaginous to rarely osseous metaplasia. There was also moderate deposition of ground substance with rare scattered mononuclear infiltrates. Angiogenesis was marked with highest density within the surgical site and extension into the adjacent tendon with increased vessel prominence throughout the tendon body. Similar to previous ovine models of tendon injury, while damage was isolated to a portion of the enthesis, pathologic changes were noted throughout the tendon body, extending distal towards the muscle belly (22).

Upon analyzing the relationship between the data collected at both the macroscopic and microscopic levels, it can be seen that the cellular activity and microstructure significantly impact the tendon mechanics. These data reveal a strong, significant relationship between the peak stress and the Bonar pathologic score ($\rho=-0.72$, *Figure 7*). As collagen is the primary load-carrying component of tendons, it is evident that pathologic scoring criteria that assess collagen organization and degeneration could predict the mechanical performance of the tendons to some degree. The relationship between tendon microstructure and mechanical competence is further bolstered by the strong, significant correlation between peak stress and the CSA of the tendons ($\rho=-0.67$, *Figure 7*). These data highlight the relationship between length-scales of the tendon—with the cell-level changes driving the ultimate functionality of the tendon.

Gene expression patterns in these tendons were changed similarly to what has been documented in literature regarding injured human rotator cuff tendons. Jelinsky *et al.* [dataset] (34) measured global gene expression patterns in diseased human tendons obtained intraoperatively; however, the main findings included Flexor-Pronator, supraspinatus and extensor carpi radialis brevis tendons, whereas the present study was controlled to a single tendon type (Accession number GSE26051). At the 12-week timepoint, the ovine tendons exhibited similar expression patterns of collagen genes compared to the human study in 21 out of the 26 collagen genes that were regulated in our study. Interestingly, this similarity dissipated at the 18-week timepoint, with only 7 out of the 26 genes matching expression patterns. Upon comparison of the lesioned supraspinatus tendon *vs.* the non-lesioned subscapularis tendon data from Jelinsky *et al.* using the GEO2R tool, (Gene Expression Omnibus (GEO), RRID:SCR_005012), out of 2,642 significant DEGs, there was a 66.7% match of gene expression pattern in our 12-week ST ovine samples (both up- or down-regulated in sheep and human datasets). This change in expression pattern between the ovine model timepoints highlights the temporal nature of tendon injury, degeneration, and healing phases. Less is known regarding the gene expression patterns of chronic tendon damage over long periods of time in humans. Ireland *et al.* (52) using RT-PCR showed that late stage degenerated Achilles tendons in humans have increased expression of type III and type I collagen, tenascin, which matches the magnitude of changes we observed in our ST model at 12-weeks. An additional study by Ireland *et al.* (52) showed upregulation of MMP-2, FNRB (ITGB1), VEGF, MAPK in chronic Achilles

tendinosis, which was also seen in similar magnitudes in the 12-week ST samples. These similarities help to strengthen our conjecture that this ST model is an appropriate translational model of human tendinopathy. Specifically, it appears that the 12-week timepoint most closely matches the gene expression pattern that has been documented in human cases of tendinopathy, thus suggesting it may be the most appropriate timepoint at which to analyze and study chronic tendon degeneration.

This study has several limitations that should be considered when interpreting the results. Most previous studies have relied on destructive biomechanical testing to benchmark the properties of injured and repaired tendons, with the general idea that improved ultimate force or stress would be correlated with improved surgical outcomes. While this reasoning is sound, destructive testing precludes the ability to perform subsequent histological analysis on the samples. This study utilized non-destructive stress relaxation testing to tease out differences in tendon mechanical properties, while still enabling subsequent histological analysis—enabling direct correlation between the mechanical properties, pathologic characteristics, and gene expression levels of the tendons at various timepoints. Unfortunately, non-destructive viscoelastic properties of degenerated human tendons have not yet been studied, rendering a comparison of changes between this model and what happens in humans intractable. A further limitation of this research is that the histological sections were scored semi-quantitatively. Although an established grading scheme was followed, exact amounts or levels of features of interest such as cellularity were not calculated. Ongoing work entails examining the non-destructive viscoelastic properties of degenerated and healthy cadaveric human tendons, followed by subsequent histopathologic, histomorphometric, and gene expression analysis—providing researchers new understanding of the relationships between macrostructural properties and the underlying microstructural arrangement and cellular activity in human samples. By better exploring the connections between the biophysical and biochemical length-scales, researchers will be enabled to better understand and develop biological therapies that will ultimately improve the prognosis of tendon repair surgeries.

This new translational model of enthesis damage is a vital step towards improving the understanding of the pathogenesis of chronic rotator cuff degeneration, laying the framework for better understanding the impact of future biologics and therapies aimed at improving tendon repair surgeries. Arguably this reproducible model is the

most accurate large animal model capable of reproducing pathologic changes similar to those witnessed in the human rotator cuff degenerative cascade. This model is especially powerful considering the similarities in size, structure, and healing capacity between sheep and humans, thus providing an effective platform with which to test new therapies and treatments for this condition. However, it is worth noting that this model fundamentally was designed to replicate degenerative changes that occur secondary to enthesis trauma. Therefore, there still is a necessity for future work to investigate the impact of mid-substance damage and to compare the way in which these two types of damage manifest in the tendon degeneration cascade.

This novel translational ovine model shows similar changes in tenocyte reactivity, angiogenesis, collagen organization, and ground substance deposition to what is seen in humans with chronic rotator cuff degeneration. Furthermore, this model was able to produce gene expression pattern changes that are similar to those documented in humans, thus lending to the accuracy and translatability of this model. Specifically, the 12-week timepoint appears to most accurately embody the characteristics of chronic tendon degeneration seen clinically. This model has the potential to improve the understanding of the underlying pathways that lead to the degenerative state seen in humans, thus providing researchers a valuable platform in which to research new treatments and therapies.

Footnote

Reporting Checklist: The authors have completed the ARRIVE reporting checklist and the MDAR checklist. Available at http://dx.doi.org/10.21037/atm-21-354

Data Sharing Statement: Available at http://dx.doi.org/10.21037/atm-21-354

Peer Review File: Available at http://dx.doi.org/10.21037/atm-21-354

Conflicts of Interest: All authors have completed the ICMJE uniform disclosure form (available at http://dx.doi.org/10.21037/atm-21-354). Dr. TR reports personal fees from Arthrex, Inc., personal fees from Atreon Orthopaedics, personal fees from Paragen, outside the submitted work. Dr. TS reports grants from Arthrex Education Grant, grants from Gemini Mountain Education Grant, outside the submitted work; and Stock/stock options in the following companies: Kaleo, PRIVIT, Avenu and NASH. The other authors have no conflicts of interest to declare.

Ethical Statement: The authors are accountable for all aspects of the work in ensuring that questions related to the accuracy or integrity of any part of the work are appropriately investigated and resolved. The study was conducted in accordance with the Declaration of Helsinki (as revised in 2013). The study was approved by institutional ethics board of the Rush Medical University (No.: 16110707-IRB01) and informed consent was taken from all individual participants. Experiments were performed under a project license (No.: 18-7854A) granted by institutional committee board of Colorado State University, in compliance with United States national or institutional guidelines for the care and use of animals.

References

1. Reilly P, Macleod I, Macfarlane R, et al. Dead men and radiologists don't lie: a review of cadaveric and radiological studies of rotator cuff tear prevalence. Ann R Coll Surg Engl 2006;88:116-21.
2. Thigpen CA, Shaffer MA, Gaunt BW, et al. The American Society of Shoulder and Elbow Therapists' consensus

Page 14 of 15

Johnson et al. Translatable model of chronic rotator cuff degeneration

statement on rehabilitation following arthroscopic rotator cuff repair. J Shoulder Elbow Surg 2016;25:521-35.

3. Fukuda H. The management of partial-thickness tears of the rotator cuff. J Bone Joint Surg Br 2003;85:3-11.

4. Matthews TJ, Hand GC, Rees JL, et al. Pathology of the torn rotator cuff tendon. Reduction in potential for repair as tear size increases. J Bone Joint Surg Br 2006;88:489-95.

5. McIntyre LF, Bishai SK, Brown PB, et al. Patient-Reported Outcomes After Use of a Bioabsorbable Collagen Implant to Treat Partial and Full-Thickness Rotator Cuff Tears. Arthroscopy 2019;35:2262-71.

6. Galatz LM, Ball CM, Teefey SA, et al. The outcome and repair integrity of completely arthroscopically repaired large and massive rotator cuff tears. J Bone Joint Surg Am 2004;86:219-24.

7. Cole BJ, McCarty LP, Kang RW, et al. Arthroscopic rotator cuff repair: Prospective functional outcome and repair integrity at minimum 2-year follow-up. J Shoulder Elbow Surg 2007;16:579-85.

8. Harryman DT 2nd, Mack LA, Wang KY, et al. Repairs of the rotator cuff. Correlation of functional results with integrity of the cuff. J Bone Joint Surg Am 1991;73:982-9.

9. Meyer M, Klouche S, Rousselin B, et al. Does arthroscopic rotator cuff repair actually heal? Anatomic evaluation with magnetic resonance arthrography at minimum 2 years follow-up. J Shoulder Elbow Surg 2012;21:531-6.

10. Longo UG, Ronga M, Maffulli N. Achilles tendinopathy. Sports Med Arthrosc Rev 2009;17:112-26.

11. Samiric T, Parkinson J, Ilic MZ, et al. Changes in the composition of the extracellular matrix in patellar tendinopathy. Matrix Biology 2009;28:230-6.

12. Ibrahim M, Kartus JT, Steigen SE, et al. More tendon degeneration in patients with shoulder osteoarthritis. Knee Surg Sports Traumatol Arthrosc 2019;27:267-75. Erratum in: Knee Surg Sports Traumatol Arthrosc. 2018 Nov 2.

13. Longo UG, Franceschi F, Ruzzini L, et al. Histopathology of the Supraspinatus Tendon in Rotator Cuff Tears. Am J Sports Med 2008;36:533-8.

14. Deprés-Tremblay G, Chevrier A, Snow M, et al. Rotator cuff repair: a review of surgical techniques, animal models, and new technologies under development Rotator cuff anatomy and pathology. J Shoulder Elbow Surg 2016;25:2078-85.

15. Gerber C, Fuchs B, Hodler J. The results of repair of massive tears of the rotator cuff. J Bone Joint Surg Am 2000;82:505-15.

16. Soslowsky LJ, Carpenter JE, DeBano CM, et al. Development and use of an animal model for investigations on rotator cuff disease. J Shoulder Elbow Surg 1996;5:383-92.

17. Grumet RC, Hadley S, Diltz MV, et al. Development of a new model for rotator cuff pathology: the rabbit subscapularis muscle. Acta Orthop 2009;80:97-103.

18. Derwin KA, Baker AR, Codsi MJ. Assessment of the canine model of rotator cuff injury and repair. J Shoulder Elbow Surg 2007;16:S140-8.

19. Gerber C, Schneeberger AG, Perren SM, et al. Experimental rotator cuff repair. A preliminary study. J Bone Joint Surg Am 1999;81:1281-90.

20. Sonnabend DH, Howlett CR, Young AA. Histological evaluation of repair of the rotator cuff in a primate model. J Bone Joint Surg Br 2010;92:586-94.

21. Turner AS. Experiences with sheep as an animal model for shoulder surgery: Strengths and shortcomings. J Shoulder Elbow Surg 2007;16:S158-63.

22. Easley J, Johnson J, Regan D, et al. Partial Infraspinatus Tendon Transection as a Means for the Development of a Translational Ovine Chronic Rotator Cuff Disease Model. Vet Comp Orthop Traumatol 2020;33:212-9.

23. Easley J, Puttlitz C, Hackett E, et al. A prospective study comparing tendon-to-bone interface healing using an interposition bioresorbable scaffold with a vented anchor for primary rotator cuff repair in sheep. J Shoulder Elbow Surg 2020;29:157-66.

24. Coleman SH, Fealy S, Ehteshami JR, et al. Chronic rotator cuff injury and repair model in sheep. J Bone Joint Surg Am 2003;85:2391-402.

25. Santoni BG, McGilvray KC, Lyons AS, et al. Biomechanical analysis of an ovine rotator cuff repair via porous patch augmentation in a chronic rupture model. Am J Sports Med 2010;38:679-86.

26. Galatz LM, Rothermich SY, Zaegel M, et al. Delayed Repair of Tendon to Bone Injuries Leads to Decreased Biomechanical Properties and Bone Loss. J Orthop Res 2005;23:1441-7.

27. Gerber C, Meyer DC, Schneeberger AG, et al. Effect of tendon release and delayed repair on the structure of the muscles of the rotator cuff: an experimental study in sheep. J Bone Joint Surg Am 2004;86:1973-82.

28. Derwin KA, Codsi MJ, Milks RA, et al. Rotator cuff repair augmentation in a canine model with use of a woven poly-L-lactide device. J Bone Joint Surg Am 2009;91:1159-71.

29. Smith MM, Sakurai G, Smith SM, et al. Modulation of aggrecan and ADAMTS expression in ovine tendinopathy induced by altered strain. Arthritis Rheum

2008;58:1055-66.

30. Melrose J, Smith MM, Smith SM, et al. Altered stress induced by partial transection of the infraspinatus tendon leads to perlecan (HSPG2) accumulation in an ovine model of tendinopathy. Tissue and Cell 2013;45:77-82.

31. Gerber C, Pennington SD, Nyffeler RW. Reverse Total Shoulder Arthroplasty. J Am Acad Orthop Surg 2009;17:284-95.

32. Vourazeris JD, Wright TW, Struk AM, et al. Primary reverse total shoulder arthroplasty outcomes in patients with subscapularis repair versus tenotomy. J Shoulder Elbow Surg 2017;26:450-7.

33. Somerson JS, Hsu JE, Gorbaty JD, et al. Classifications in Brief: Goutallier Classification of Fatty Infiltration of the Rotator Cuff Musculature. Clin Orthop Relat Res 2016;474:1328-32.

34. Jelinsky SA, Rodeo SA, Li J, et al. Regulation of gene expression in human tendinopathy. BMC Musculoskelet Disord 2011;12:86.

35. Noyes FR, Butler DL, Grood ES, et al. Biomechanical analysis of human ligament grafts used in knee-ligament repairs and reconstructions. J Bone Joint Surg Am 1984;66:344-52.

36. McGilvray KC, Santoni BG, Turner AS, et al. Effects of 60Co gamma radiation dose on initial structural biomechanical properties of ovine bone—patellar tendon—bone allografts. Cell Tissue Bank 2011;12:89-98.

37. McGilvray KC, Lyons AS, Turner AS, et al. Shoulder Tendon Repair Biomechanics Using a Polyurethane Patch in a Chronic Ovine Defect Model. Am Soc Mech Eng 2007;(47985):853-4.

38. France EP, Paulos LE, Harner CD, et al. Biomechanical evaluation of rotator cuff fixation methods. Am J Sports Med 1989;17:176-81.

39. Schlegel TF, Hawkins RJ, Lewis CW, et al. The Effects of Augmentation with Swine Small Intestine Submucosa on Tendon Healing under Tension. Am J Sports Med 2006;34:275-80.

40. Rodeo SA, Arnoczky SP, Torzilli PA, et al. Tendon-healing in a bone tunnel. A biomechanical and histological study in the dog. J Bone Joint Surg Am 1993;75:1795-803.

41. Sverdlik A, Lanir Y. Time-Dependent Mechanical Behavior of Sheep Digital Tendons, Including the Effects of Preconditioning. J Biomech Eng 2002;124:78-84.

42. Troyer KL, Puttlitz CM. Nonlinear viscoelasticty plays an essential role in the functional behavior of spinal

ligaments. J Biomech 2012;45:684-91.

43. Paxton JZ, Hagerty P, Andrick JJ, et al. Optimizing an Intermittent Stretch Paradigm Using ERK1/2 Phosphorylation Results in Increased Collagen Synthesis in Engineered Ligaments. Tissue Eng Part A 2012;18:277-84.

44. Liao J, Vesely I. Relationship Between Collagen Fibrils, Glycosaminoglycans, and Stress Relaxation in Mitral Valve Chordae Tendineae. Ann Biomed Eng 2004;32:977-83.

45. Cook JL, Feller JA, Bonar SF, et al. Abnormal tenocyte morphology is more prevalent than collagen disruption in asymptomatic athletes' patellar tendons. J Orthop Res 2004;22:334-8.

46. Sikes KJ, Li J, Gao SG, et al. TGF-b1 or hypoxia enhance glucose metabolism and lactate production via HIF1A signaling in tendon cells. Connect Tissue Res 2018;59:458-71.

47. Kim D, Pertea G, Trapnell C, et al. TopHat2: accurate alignment of transcriptomes in the presence of insertions, deletions and gene fusions. Genome Biology 2013;14:R36.

48. Hee CK, Dines JS, Dines DM, et al. Augmentation of a Rotator Cuff Suture Repair Using rhPDGF-BB and a Type I Bovine Collagen Matrix in an Ovine Model. Am J Sports Med 2011;39:1630-9.

49. Sethi PM, Sheth CD, Pauzenberger L, et al. Macroscopic Rotator Cuff Tendinopathy and Histopathology Do Not Predict Repair Outcomes of Rotator Cuff Tears. Am J Sports Med 2018;46:779-85.

50. Nakajima T, Rokuuma N, Hamada K, et al. Histologic and biomechanical characteristics of the supraspinatus tendon: Reference to rotator cuff tearing. J Shoulder Elbow Surg 1994;3:79-87.

51. Roßbach BP, Gülecyüz MF, Kempfert L, et al. Rotator Cuff Repair With Autologous Tenocytes and Biodegradable Collagen Scaffold: A Histological and Biomechanical Study in Sheep. Am J Sports Med 2020;48:450-9.

52. Ireland D, Harrall R, Curry V, et al. Multiple changes in gene expression in chronic human Achilles tendinopathy. Matrix Biol 2001;20:159-69.